J. Fluid Mech. (1988), *vol.* 192, *pp.* 577–595
Printed in Great Britain

The structure of a shear layer bounding a separation region. Part 2. Effects of free-stream turbulence

By I. P. CASTRO† AND A. HAQUE‡

† Department of Mechanical Engineering, University of Surrey, Guildford, Surrey, GU2 5XH, UK

‡ Department of Chemical Engineering, Imperial College, London, SW7 2AZ, UK

(Received 19 June 1987 and in revised form 21 December 1987)

Detailed measurements throughout the separated region behind a flat plate placed normal to a turbulent stream are reported. A long, central, downstream splitter plate prevented vortex shedding and led to a relatively extensive reversed flow region. Mean flow and turbulence data are compared with results obtained in the (nominal) absence of free-stream turbulence, and attention is concentrated on the changes in the shear-layer structure resulting from the different nature of the upstream flow.

Many aspects of the results confirm those obtained recently by other workers. Free-stream turbulence enhances shear-layer entrainment rates, reduces the distance to reattachment and modifies the relatively low-frequency 'flapping' motion of the shear layer. In addition, however, extensive use of pulsed wire anemometry has allowed detailed measurements of the turbulence structure throughout the flow and it is shown that this is also modified significantly by the stream turbulence.

1. Introduction

Many flows of engineering importance contain separated regions bounded by a turbulent stream. Typical examples occur, for example, in the wind engineering context where the highly-turbulent reversed-flow regions in the lee of buildings occur deep within a surrounding turbulent atmospheric boundary layer. The controlled regions of separation which may occur on multi-element aerofoils, in turbomachinery and in diffusers of many kinds, can also lie beneath an essentially turbulent outer flow. Whilst many studies have documented the effects of free-stream turbulence on ordinary shear flows, relatively little is known about how turbulence affects the development and structure of separated flows. This is no doubt largely because understanding of even the simplest turbulent separated flow is much less well developed than that of classical shear flows.

Wall boundary layers (e.g. Hancock & Bradshaw 1983) and two-stream mixing layers (e.g. Pui & Gartshore 1979; Patel 1978) can be significantly modified by free-stream turbulence. Generally speaking, mean flow growth rates and turbulence Reynolds stresses are all enhanced if the lengthscale of the free-stream turbulence is of a similar order to the shear flow scales. Now a two-dimensional separated flow must always be bounded by two strongly sheared regions, at least one of which separates the reversed flow from the outer streaming flow and is qualitatively rather like a plane mixing layer (but see below). One might therefore expect separated regions to respond in at least some way to outer flow turbulence, via the latter's

influence on the separated shear layer. In fact, it is well known that the axial extent of the separated region can be substantially reduced by free-stream turbulence. This has been most clearly demonstrated in the context of bluff-body flows, where the additional turbulence 'invigorates' the separated shear layers (Bearman & Morel 1983). In free flows this can sometimes lead to their reattachment onto the sides of the obstacle, with consequent changes in, say, the vortex shedding process. In the case of flow around surface mounted (or long) obstacles, reattachment can occur significantly earlier than it would in the absence of free-stream turbulence. Hillier & Cherry (1981), for example, showed that the separated regions on the sides of a long blunt plate contracted monotonically with increasing free-stream turbulence intensity. This was accompanied by a decrease in the separation pressure coefficient. Fluctuating surface pressures were affected in ways dependent on both free-stream intensity and lengthscale and the dependence was shown to be markedly different in different regions of the flow field. Similar results were obtained recently for the same geometry by Nakamura & Ozono (1987). They showed that the mean pressure variation along the surface of the body is insensitive to free-stream turbulence integral scale unless the latter exceeds twice the body thickness.

However, the change in size of the separated region is an overall effect and whilst it can be plausibly explained on the assumption that turbulence stresses and mean flow growth rates of the separated shear layer increase with the addition of free-stream turbulence, there is no detailed evidence that this is, in fact, the cause. Indeed, the detailed response to free-stream turbulence of a shear layer bounding a separated region remains an open question. As Hillier & Cherry stated, 'the mechanisms of the interaction between stream turbulence and the shear layer are unclear'. One of the major purposes of the work presented here was to obtain detailed measurements within the separated shear layer so that direct comparisons with data obtained in the case of very low free-stream turbulence could be made. This has not been done before.

In the companion paper to this, Castro & Haque (1987) (hereinafter referred to as CH) presented detailed measurements made throughout the separated region behind a flat plate normal to a uniform, laminar stream. The plate (height $2H$) was fitted with a long, downstream, central splitter plate so that vortex shedding was suppressed. Reattachment of the shear layers occurred about $17H$ downstream. This flow, whilst geometrically simple, is fluid dynamically more complex than the much studied backstep configuration, and has features more akin to those of typical bluff-body flows. It was shown that the shear layer had characteristics quite unlike those of an ordinary plane mixing layer. In particular, its growth rate is neither closely linear nor equal to that of the plane mixing layer, the maximum turbulence energy rises continually up to reattachment, and turbulence structure parameters have a cross-stream behaviour and axial development quite different to that in the ordinary plane mixing layer. In this paper we present and discuss results of a similar experiment conducted in a turbulent free stream, concentrating on the general questions of how, and to what extent, the turbulence characteristics are modified by the presence of the free-stream turbulence.

Ordinary grid generated turbulence was used for the latter and we chose a configuration that gave a free-stream longitudinal integral scale of about $1.3H$ at the plate position, rising to about $1.6H$ near reattachment. As far as the overall flow is concerned, it has become clear from earlier work that where separation at large angles to the approach flow occurs (90° in the present case) the free-stream lengthscale is not a dominant parameter (e.g. Bearman & Morel 1983), provided it is

sufficiently small (less than $4H$ according to Nakamura & Ozono 1987). However, the above values would be typical of the integral scales occurring near the body height in the case of obstacles immersed in thick turbulent boundary layers. The 'outer' turbulence then inevitably has scales much larger than those in the separated shear layer just after separation, but as reattachment is approached the shear-layer lengthscales become more comparable with those in the outer flow. In the present experiment the longitudinal turbulent intensity fell from about $3\frac{1}{2}$ to 3% over the length of the reversed flow region. These levels are much smaller than would be typical in the above situation but are of the same order as those used in investigations of free-stream turbulence effects on plane mixing layers. Any really substantial increase (in excess of a factor of two, say) would require the turbulence generating grid to be placed much nearer the flat plate; this would inevitably be accompanied by a wider variation in both intensity and scale over the length of the separated region and, probably, rather more spanwise inhomogeneity in the flow. (Lateral homogeneity in grid generated turbulence generally only occurs for $x/M > 10$, say, where M is the mesh size; mean flow inhomogeneities would be strongly amplified by the strong pressure gradients just upstream of the normal plate.)

2. Experimental arrangements

A detailed description of the experimental arrangements is given in CH. The only difference in the present case was provision of the turbulence generating grid. This was a square mesh biplanar type and was mounted nominally $33H$ upstream of the flat plate. Standard hot-wire measurements downstream of the grid and in the absence of the plate showed that over the axial region spanned by the latter plus its separated wake the longitudinal turbulence intensity decayed according to:

$$(\overline{u^2}/U^2)^{-0.8} = 8.1(x'/M - 5.8),$$

where x' is measured from the grid position and M is the mesh spacing (50 mm). Crossed-wire measurements showed that the degree of anisotropy was within the typical ranges found by other workers for this type of grid (e.g. Compte-Bellot & Corrsin 1966). Longitudinal velocity autocorrelation measurements led, via Taylor's hypothesis, to an integral scale given by:

$$L_x/M = 0.015(x'/M + 10.4).$$

With the assumption that L_x grows at a rate proportional to the growth of the dissipation length parameter, $L_\epsilon = (\overline{q^2})^{\frac{3}{2}}/\epsilon$, this result is not really consistent with the above decay of $\overline{u^2}$. However, these expressions fitted the experimental data well over the limited but appropriate range $33 < x'/M < 55$ and are adequate for the present purpose. Note again that this arrangement led to a free-stream turbulence scale of 0.65 plate heights ($2H$) at the plate position; this is well within the range quoted by Nakamura & Ozono (1987) for which they found no significant effect of turbulence scale (on wall static pressures at least). Further details of the free-stream turbulence are available from the first author.

Figure 1 is a sketch of the overall set-up of the 6 mm thick flat plate spanning the shorter width of the 0.77×0.62 m working section of the blow-down low-speed wind tunnel in the Mechanical Engineering Department. The plate height was 50 mm and the 3 mm thick splitter plate extended downstream a distance of about $35H$. This contained instrumentation ports at regular intervals along its centreline, for the convenient insertion of the surface static pressure taps or skin friction probes. No

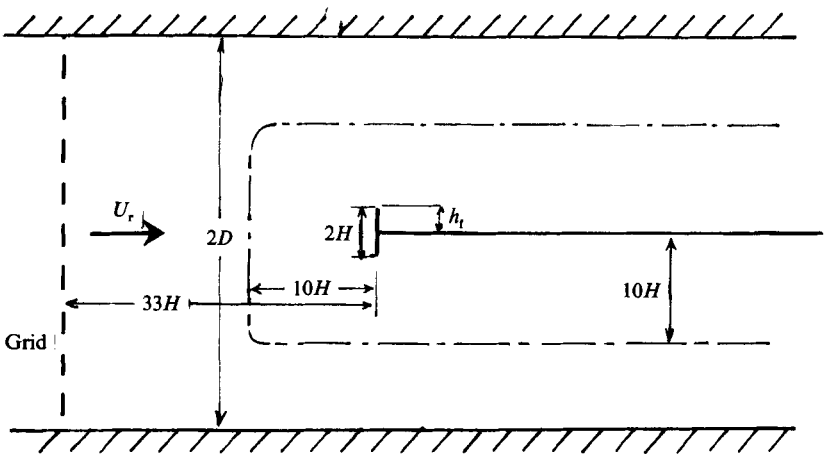

FIGURE 1. Experimental arrangement; not to scale.

corrections for the effect of wind-tunnel blockage have been attempted in the present work, since it seems unlikely that the latter can significantly alter the effects produced by free-stream turbulence. In the present case, H/D was about 8%, where D is the tunnel half height (figure 1); presumably only when $L_x/H = O((D-H)/H)$ would blockage become an important parameter as far as changes in the effects of free-stream turbulence are concerned. CH includes a brief discussion and comparison of the overall flow for different blockage ratios.

End plates were fitted as described by CH; these ensured an adequate two-dimensionality of the flow. In fact, it is interesting that the two-dimensionality was noticeably improved, in one respect at least, by the addition of free-stream turbulence. Figure 2 shows the spanwise location of the mean reattachment line, normalized by the centreline value and compared with the equivalent result in the absence of free-stream turbulence. A similar effect has been noted previously (e.g. Hillier & Cherry 1981) and it seems that the free-stream turbulence affects the production and/or development of the strong vortices at the junction between the normal plate and the endwalls. Their influence is certainly weaker than it is in the absence of free-stream turbulence.

Extensive use was made of pulsed-wire anemometry, both for measurements within the flow itself and for the determination of wall skin friction. Full details are given in CH, but it is worth emphasizing here that the design of the pulsed-wire probes was optimized to ensure as accurate a determination of the Reynolds normal and shear stresses as possible. The major feature of the probe geometry, as discussed in CH, was that the plane containing the sensor wires was inclined at about 30° to the axis of the pulsed wire. Wire spacings and lengths were 1.25 and 9 mm, respectively, and the resulting yaw response was accurately cosinusoidal up to flow angles of $\pm 80°$. It was concluded in CH that measurements of the Reynolds stresses were likely to be at least as accurate as those obtained using crossed hot wires in flows where such probes can be sensibly used. The wall skin friction probe, discussed by Castro & Dianat (1983), had pulsed and sensor wire lengths of 3 and 2 mm, respectively, positioned 0.025 mm above the surface and with spacings of 1.25 mm; its yaw response was very similar to the probe described above.

In the following presentation of the experimental results less emphasis (than in CH) is placed on the detailed examination of the raw data. On their own, these add

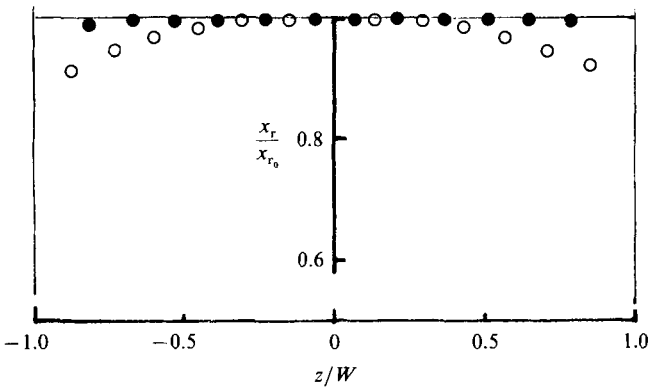

FIGURE 2. Mean reattachment line. ○, no FST; ●, with FST. $2W$ is the spacing between the endplates.

little more to the understanding of the recirculating flow than was gained by our earlier study. Rather, since the purpose is to obtain a better understanding of the influence of free-stream turbulence on a separated flow, we concentrate on direct comparisons between the two cases. Nonetheless, the data do have some implications concerning the basic nature of the flow and discussion of these are included as appropriate in later sections. For conciseness, free-stream turbulence is hereinafter denoted by FST.

3. The mean flow

Figures 3 and 4 present the distributions of static pressure and skin friction, respectively, on the splitter-plate surface, compared with those obtained in the absence of stream turbulence. C_p is defined by $(p-p_r)/\frac{1}{2}\rho U_r^2$, where suffix r refers to conditions in the free stream about $20H$ upstream. Similarly, $C_f = \tau_w/\frac{1}{2}\rho U_r^2$, where τ_w is the surface shear stress. The Reynolds number, defined by $Re = 2HU/\nu$, was about 2.3×10^4 in both cases. As found by CH, measurements at different (lower) Re demonstrated that C_p was virtually independent of Re over the range covered, whereas C_f was certainly not. It was shown in CH that plotting τ_w normalized using U_N, the minimum (negative) velocity at the particular x-station, against a Reynolds number based on U_N and the distance from the mean reattachment point, collapsed the present data (with and without FST) with the other published results for C_f in separated flows. They argued that overall flow geometry is not dominant in determining the development of the thin boundary layer beneath a separated region. Free-stream turbulence only affects this development through its influence on U_N.

Renormalizing the wall static pressure data using a pressure coefficient of the form:

$$\tilde{C}_p = (C_p - C_{pmin})/(1 - C_{pmin}),$$

(Roshko & Lau 1965) collapses the two sets of data when plotted against x/x_R. (x_R is the distance to reattachment.) However, the base pressure is clearly rather lower in the presence of FST and the subsequent pressure recovery is significantly more rapid, with reattachment occurring at $x/h_f = 14.8$. (Note that h_f, defined in figure 1, is the difference between the plate half-height, H, and the half-thickness of the splitter plate.) This location was checked using a twin-tube probe (Castro & Fackrell 1978) and is also consistent with the mean velocity measurements. It represents a

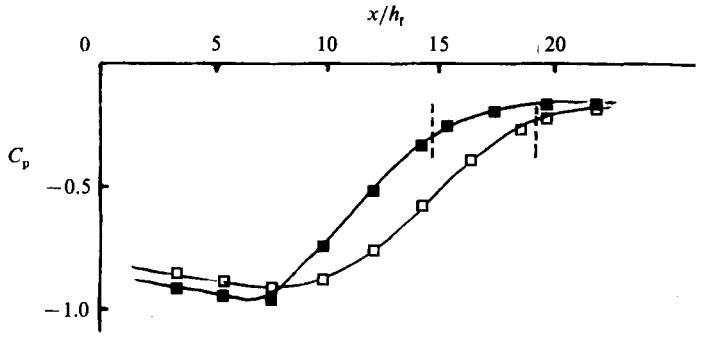

FIGURE 3. Surface static pressure distribution. □, no FST; ■, with FST. The vertical dashed lines indicate the reattachment locations in the two cases.

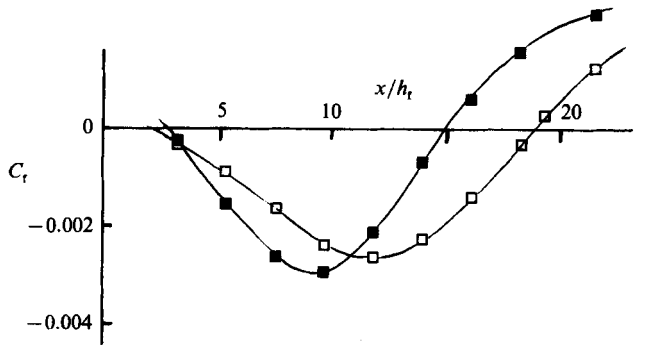

FIGURE 4. Surface skin friction distribution. □, no FST; ■, with FST.

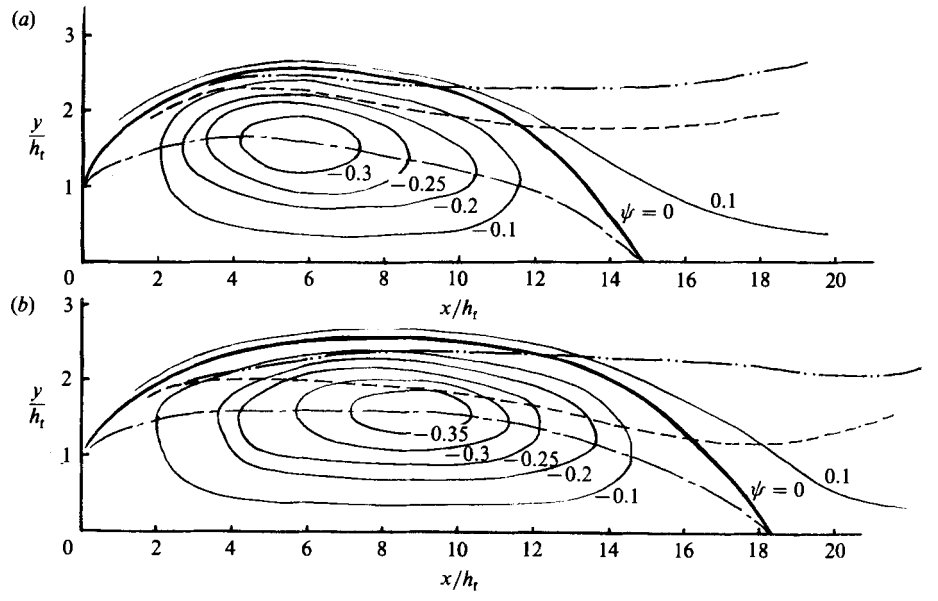

FIGURE 5. Mean streamlines (*a*) with and (*b*) without FST. ————, line of maximum $\overline{u^2}$; – – – –, $U = 0$; ·· ——— ··, $\eta = 0$; values of streamfunction, ψ, are indicated.

decrease of about 20% from the uniform free-stream case ($x_R/h_f = 18.2$), which is close to that expected from the data of Bearman (1978), who measured x_R as a function of free-stream intensity for a very similar configuration.

The mean velocity profiles were similar in form to those presented in CH; figure 5 shows streamlines deduced from them, along with the line along which $U = 0$. It is significant that the minimum value of the streamfunction, defined by

$$\psi = \int_0 U/U_r \, dy,$$

is about -0.34 (around $x/h_f = 6$), compared with about -0.39 (around $x/h_f = 9$) in the absence of FST. (y is here and henceforth normalized by h_f.) There is therefore a lower mass flux into the front half of the separated region which implies that rather less fluid is returned around reattachment. Now, as indicated earlier, it is sometimes argued that FST, by causing increased entrainment into the shear layer, actually increases the quantity of returned fluid, thereby causing earlier reattachment. The present results show that, in fact, earlier reattachment is associated with a reduction in the quantity of fluid recirculated.

Overall entrainment rates are, nonetheless, increased by FST. In terms of an entrainment rate 'per unit surface area', on the low velocity side of the layer the above figures imply an increase of some 17% in the present case. Figure 6 shows the growth of the vorticity thickness, Λ, defined by:

$$\Lambda = \left[\frac{\partial(U/\Delta U)}{\partial y}\right]^{-1}_{\max},$$

where ΔU is $(U_{\max} - U_{\min})$, the total velocity difference across the shear layer. The growth rate is noticeably higher with FST, although the overall feature of a growth rate gradually decreasing all the way to reattachment is preserved.

As in CH, we define the shear layer centreline as $\eta = 0$, the point ($y = y_c$) where the mean velocity is $(0.67\Delta U + U_{\min})$, where $U_{\min}$ is the minimum velocity on the low-speed side of the layer; $\eta = -(y_c - y)/\Lambda$. A measure of the thickness of the high- and low-velocity sides of the shear layer is then provided by $\Delta y_H = (y_{0.95} - y_{0.67})$ and $\Delta y_L = (y_{0.67} - y_{0.2})$, respectively, where y_α is the point at which the velocity is $(\alpha\Delta U + U_{\min})$. Figure 7 shows the thickness ratio, $\Delta y_H/\Delta y_L$, plotted against x/x_R for both flows. The results indicate that stream turbulence leads to a relatively faster growth of the low-velocity side (compared to that of the high-velocity side) than that which occurs in the absence of FST. It might have been expected that FST would have more effect on entrainment rates on the high-velocity side of the layer. However, this division of the shear layer, using the 0.2, 0.67 and 0.95 velocity points, is somewhat arbitrary. The 0.2-point happens to coincide roughly with the position at which the axial velocity is zero, over much of the flow. By using ΔU as the reference velocity, practically all the backward moving fluid is being included in the total shear-layer thickness. In this sense, therefore, it is perhaps not sensible to talk of this fluid being entrained into the shear layer.

Although Wygnanski & Fiedler (1970) showed that in the ordinary plane mixing layer the movements of the turbulent/non-turbulent interfaces on either side of the layer are not well correlated, there is plenty of evidence in the literature for the existence of eddies of a size comparable with the shear-layer thickness. Even when these are clearly not the strongly two-dimensional motions first identified by Brown & Roshko (1974) – as in Pui & Gartshore's (1979) experiment, for example – they must have a significant influence on the entrainment process on both sides of the

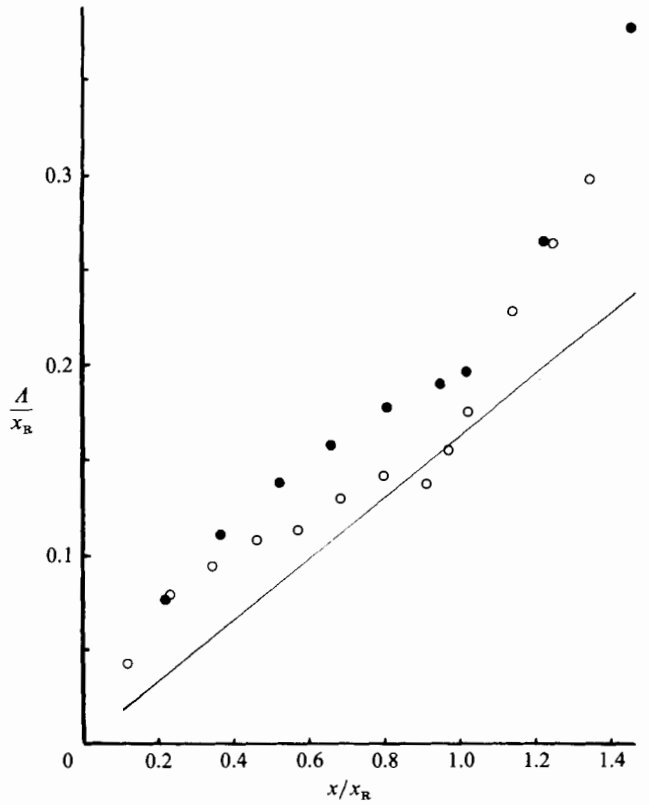

FIGURE 6. Growth of the vorticity thickness. ○, no FST; ●, with FST; ——, plane mixing layer (arbitrary origin).

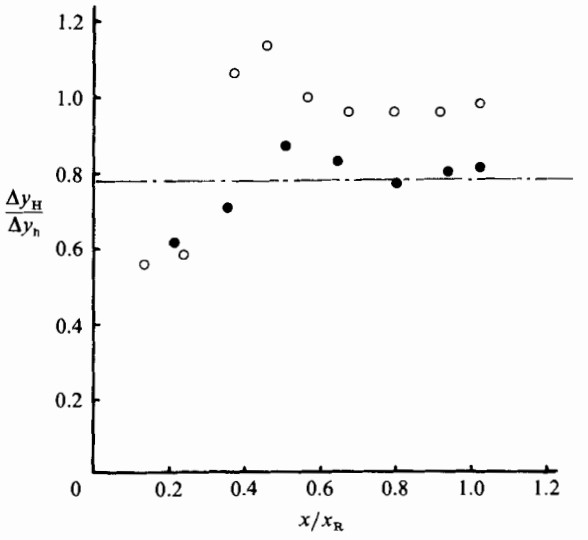

FIGURE 7. Development of the thickness ratio. ○, no FST; ●, with FST; ——, plane mixing layer value.

layer. In the present case there are, in addition, very low-frequency timescales (see Kiya & Sasaki 1983; Cherry, Hillier & Latour 1984; CH) which possibly arise from a large-scale 'bursting' of the bubble. Entrainment should therefore not be viewed as a process which occurs on both sides of the flow quite independently. It is perhaps inappropriate to conceptualize the shear layer simply as a high-velocity region, affected by entrainment from the possibly turbulent outer flow, and a low velocity region, affected by entrainment of the reversed flow beneath it. We return to this point later.

4. The turbulence structure

As in the case of the mean velocity, profiles of the Reynolds stresses were very similar to those obtained in the absence of FST, reported by CH. They will not be presented in detail. A few typical profiles are compared in figure 8 with others obtained in the earlier study. The results are plotted against η, for ease of comparison with plane mixing-layer data. Figure 9 shows the axial development of the maximum cross-stream value of each Reynolds stress, again compared with those obtained in the absence of FST. Qualitatively, the behaviour is very similar in the two cases, with peak values of all stresses occurring around reattachment – the location of the latter is included in figure 9. The major difference appears in the case of the normal component, $\overline{v^2}$, whose maximum value is significantly less than that found in the absence of FST. Possible reasons for this behaviour are discussed later, but note that rotating the stresses into coordinate axes aligned with the local direction of the shear layer (see CH) would accentuate this difference.

Turning to the cross-stream profiles in figure 8, note first that at a given axial station (x/h_f) the longitudinal component, $\overline{u^2}$, is larger across the whole flow in the presence of FST – compare the solid symbols (for $x/h_f = 7.8$, 9.9) with the open symbols (for $x/h_f = 8.9$). By contrast, the FST does not cause a corresponding increase in the other components on the high-velocity side of the flow. This could be evidence that the FST simply acts to 'flap' the separated layer laterally; in principle all the normal stresses would respond to such flapping, but by far the most dominant effect will be on the axial component because of the 'shaking' of the mean velocity gradient. Further discussion of this point is deferred to §§5 and 6, where timescales and lengthscales are considered.

Secondly, on the low-velocity side of the layer all the stresses at a given x/h_f are higher than in the absence of FST. In terms of a fixed x/x_R, however, they are a little lower – compare the solid and open symbols for the data near $x/x_R = 0.66$ in figure 8. Figure 10 shows that this is only true in the second half of the bubble. The total turbulent energy, $\overline{q^2}$, at a fixed y/h_f (1.06) well within the separated region is plotted against both x/h_f and x/x_R; note that in the latter case (figure 10*b*) $\overline{q^2}$ only begins to fall below its value in the absence of FST for $x/x_R > 0.5$. The raw turbulence energy profiles close to reattachment are compared in figure 11 and it is clear that the lower part of the shear layer contains noticeably less energy in the FST case. Since the bulk of the fluid returned upstream will presumably originate in this region it is not, perhaps, surprising that although FST increases energy levels in the outer part of the flow, $\overline{q^2}$ for $x < x_R$ in much of the bubble is lower.

The difference in response to FST of the various stress components is emphasized by the individual profiles at reattachment, shown in figure 12 plotted against η. Whilst $\overline{w^2}$ is largely unaffected, the opposite behaviour of $\overline{u^2}$ and $\overline{v^2}$ is quite apparent, with $\overline{u^2}$ now larger and $\overline{v^2}$ smaller over the whole flow in the presence of FST (cf.

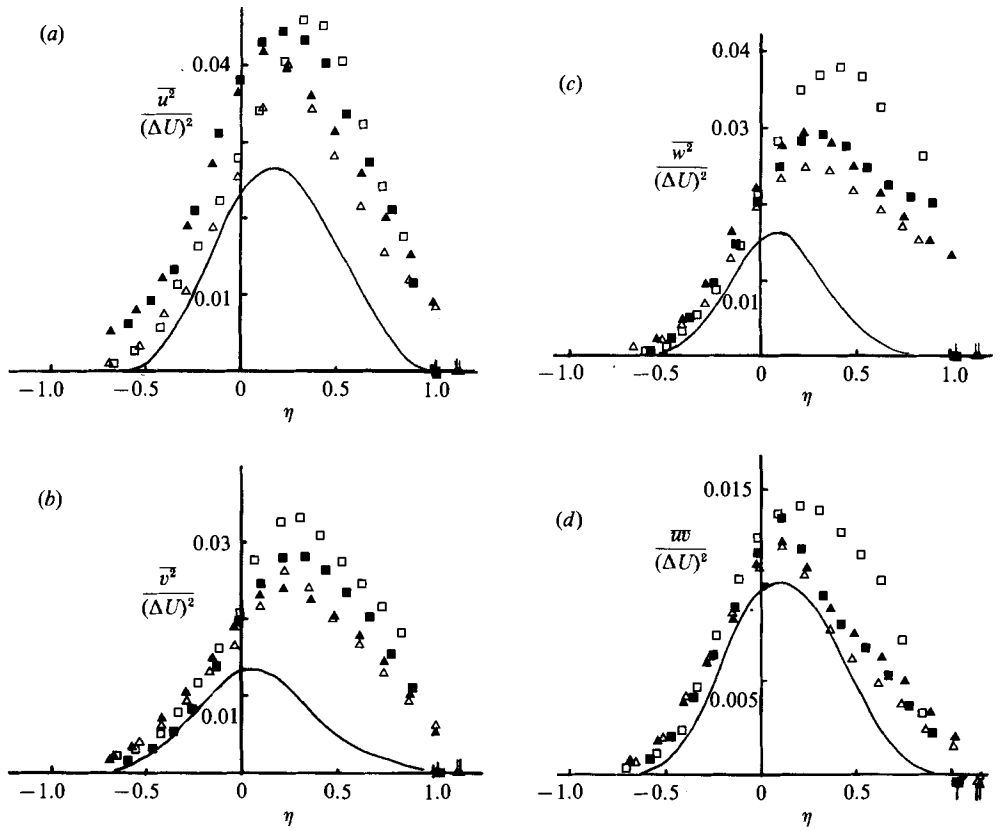

FIGURE 8. Reynolds stress profiles at $(x/h_f, x/x_R)$: □, (13.1, 0.68); ■, (9.9, 0.65); △, (8.9, 0.45); ▲, (7.8, 0.51). Solid and open symbols are with and without FST, respectively. ——, plane mixing layer. Wall locations are indicated on the η axis. (*a*) $\overline{u^2}$; (*b*) $\overline{v^2}$; (*c*) $\overline{w^2}$; (*d*) $\overline{uv}$.

figure 8 for $x/x_R = 0.65$). CH argued that the re-entrainment of returned fluid provides the possibility of 'positive feedback'. If there is any mechanism tending to amplify turbulence energy upstream of reattachment, the returned fluid will have a higher energy which, via its entrainment by the upstream flow, will further enhance the energy levels. The influence of the wall may initially be to increase the normal stress component (Wood & Bradshaw 1982) but its amplification via feedback will be limited because the wall must eventually act to reduce it. The lateral component, however, is free to continue rising relative to $\overline{v^2}$ across the whole layer. This provided a plausible explanation for the behaviour of the stress components in the absence of FST. Now in the present case, since reattachment occurs earlier, the effects of such feedback should be seen earlier (smaller x/h_f). One might also anticipate an earlier saturation in $\overline{v^2}$. The results in figures 9 and 12 have those features, which provides some further confirmation of the above arguments.

Examples of the behaviour of the structure parameters, $\overline{uv}/\overline{q^2}$, $\overline{v^2}/\overline{u^2}$ and $\overline{w^2}/\overline{u^2}$ are given in figure 13(*a*) for $x/x_R = 0.65$ and figure 13(*b*) for $x/x_R = 1.02$. These emphasize the great differences between the ordinary plane mixing layer and separated shear layers bounding a reversed flow region – discussed in detail by CH. They also highlight the fact that it is the axial stress component which is increased most in the outer region of the flow by FST. Both $\overline{v^2}/\overline{u^2}$ and $\overline{w^2}/\overline{u^2}$ are always considerably lower in the outer region than they are in the absence of FST, although

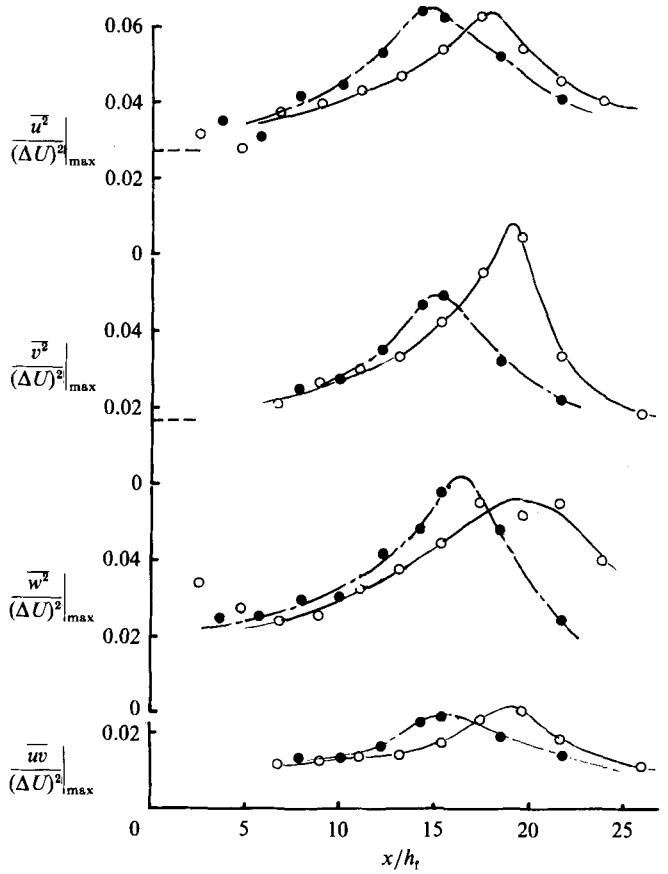

FIGURE 9. Axial development of the maximum Reynolds stresses. Note origin shifts. ○, no FST; ●, with FST; ————, plane mixing layer values.

sufficiently far out they should of course return to values close to unity.† On the low-velocity side, both parameters remain much higher than they are in a plane mixing layer, although FST leads to a more significant drop in $\overline{v^2}/\overline{u^2}$ than occurs in $\overline{w^2}/\overline{u^2}$, as anticipated from the results presented earlier.

It is also worth noting that there are significant increases in surface skin friction fluctuation levels in the presence of FST. Figure 14 compares the results obtained in both cases (for a single Reynolds number). Like the mean skin friction, c_f' is actually Reynolds number dependent, but other results not presented here showed that the proportional increase caused by FST is not. It is interesting to compare this increase with the increases in fluctuating surface pressure caused by FST, measured by Hillier & Cherry (1981). If the latter is normalized by a dynamic head based on the separation velocity $(1-C_{pb})$, these authors showed that the increase is largely independent of free-stream intensity but grows monotonically with increasing ratio of the free-stream integral lengthscale to the distance to reattachment (L_x/x_R). Figure 15 shows the increases in maximum $c_p'/(1-C_{pb})$ plotted against L_x/x_R and includes the single point available from the present experiment for the corresponding

† A referee has emphasized this last point and also reminded us that in the absence of FST, the increasing $\overline{v^2}/\overline{u^2}$ as η decreases cannot continue indefinitely, since $\overline{v^2} = \overline{u^2}+\overline{w^2}$ in the potential flow outside the shear layer (see Wood & Ferziger 1984).

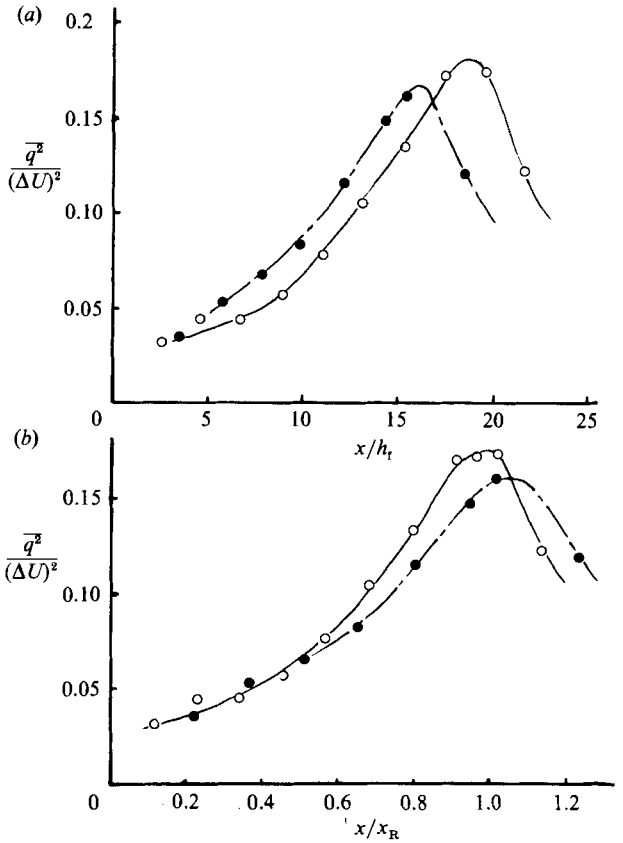

FIGURE 10. Turbulence energy along $y/h_t = 1.06$. ○, no FST; ●, with FST.

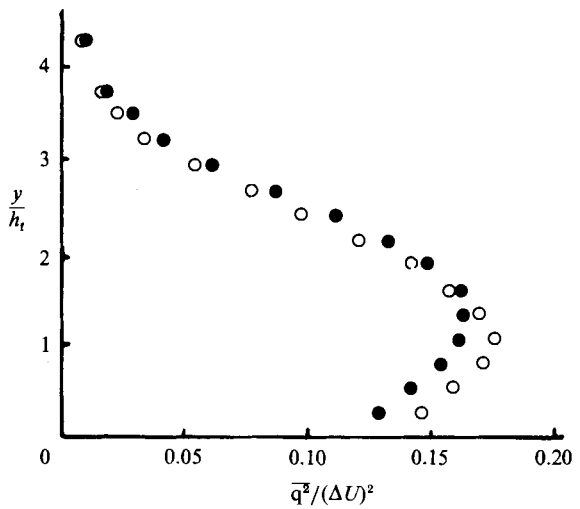

FIGURE 11. Turbulence energy profiles at reattachment ($x/x_R = 1.0$). ○, no FST; ●, with FST.

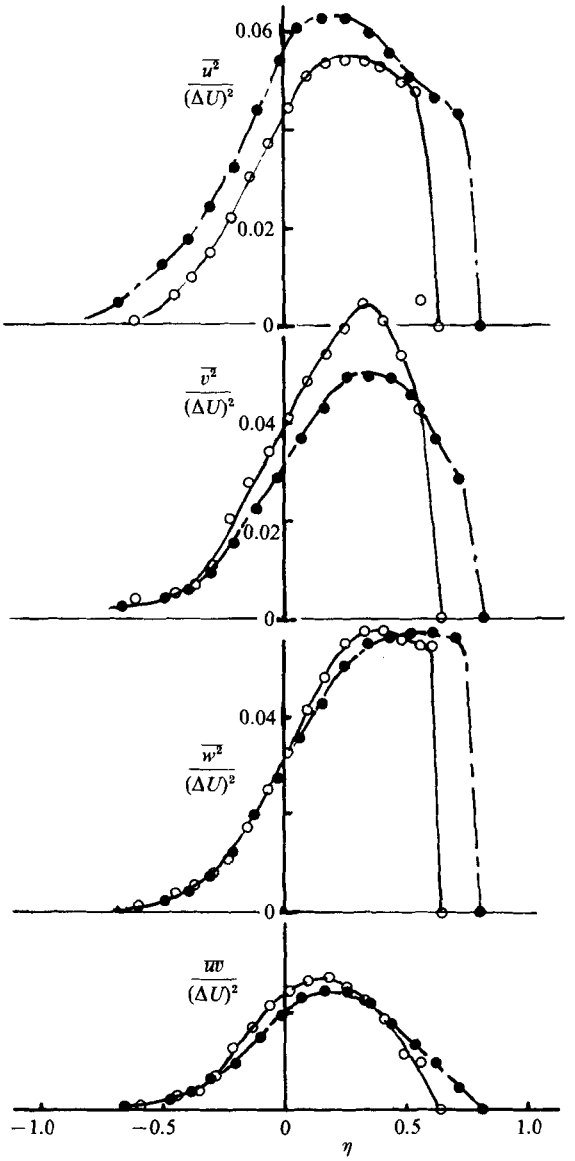

FIGURE 12. Reynolds stress profiles at reattachment. ○, no FST; ●, with FST. Wall locations correspond to zero values on the η-axis.

increase in c'_{fmax}. c'_{p} and c'_{f} are the r.m.s. fluctuating values of the instantaneous surface pressure and skin friction, respectively, normalized in the same way as the corresponding mean values. Whilst one might not expect an exact correspondence, provided the c_{f} fluctuations are essentially a result of the large-scale motions around reattachment, increases in c'_{p} do imply similar increases in c'_{f} via the Poisson equation for pressure at the wall. Our c'_{f} data is certainly consistent with the trend in Hillier & Cherry's c'_{p} data. One would also expect the increase in c'_{f} caused by FST to be a function of the free-stream turbulence intensity; more work is required to explore these points thoroughly.

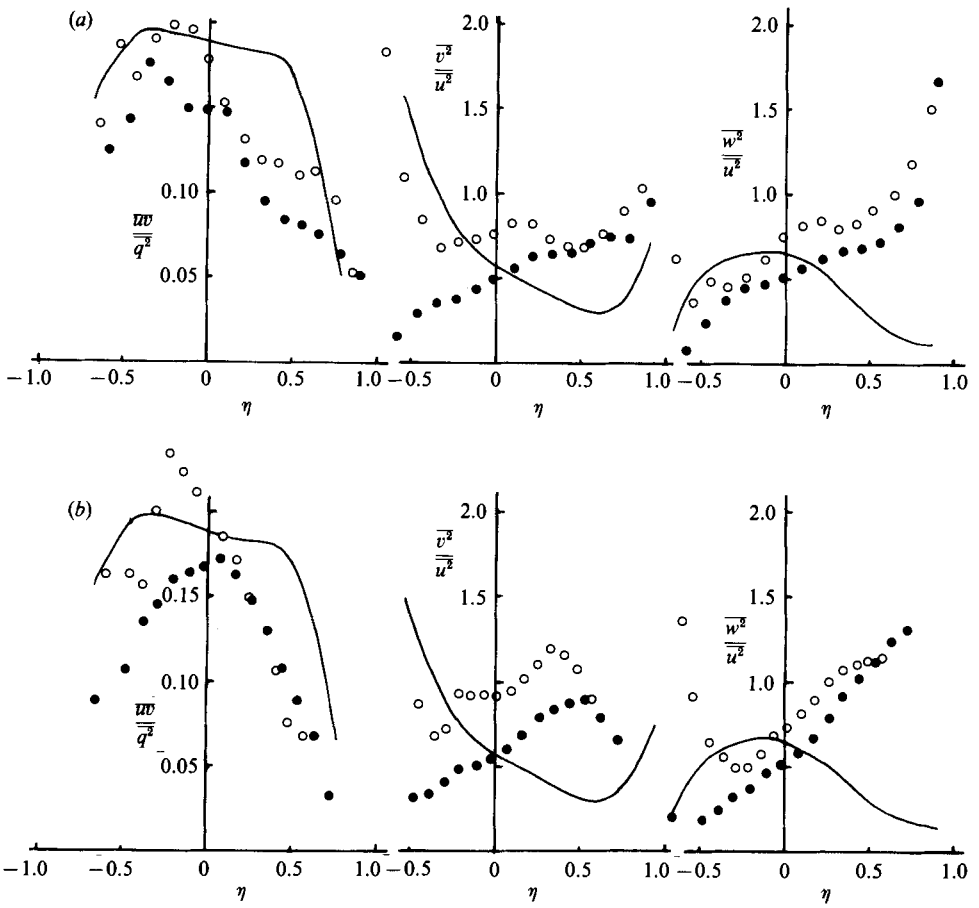

FIGURE 13. Turbulence structure functions. ○, no FST; ●, with FST; ——, plane mixing layer. (*a*) $x/x_R = 0.65$; (*b*) $x/x_R = 1.0$.

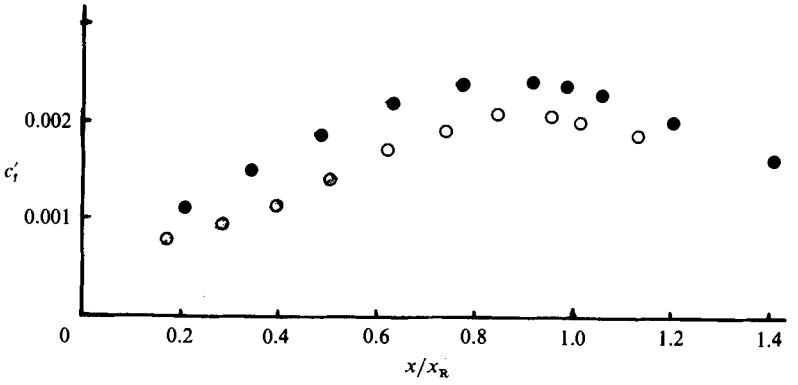

FIGURE 14. Fluctuating surface skin friction. ○, no FST; ●, with FST.

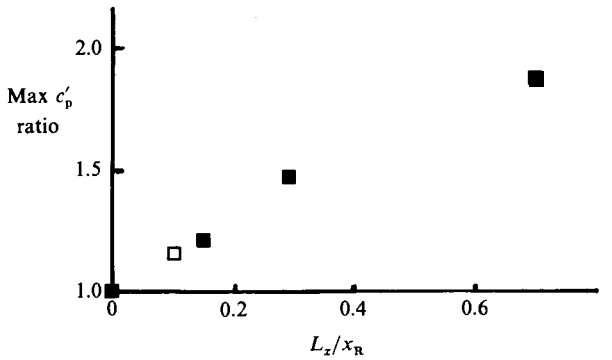

FIGURE 15. Increase in maximum $c_p'/(1-C_{pb})$, expressed as the ratio of values with and without FST (from Hillier & Cherry 1981) or c_f' (□, present result) as a function of FST integral lengthscale.

5. Timescales

Velocity autocorrelations were obtained in the separation region using pulsed-wire anemometry (Castro 1985) and the results used to estimate integral timescales, defining the latter by:

$$T_x = \int_0^{\tau'} R(\tau)\,\mathrm{d}\tau, \tag{1}$$

where τ' is the location of the first zero crossing ($\tau' = \infty$ if $R(\tau)$ tends monotonically to zero). Figure 16 shows the variation of $T'_u = T_x U_r/x$ at three stations, compared with those obtained in the absence of FST. It is immediately apparent that the peak values are significantly reduced by FST. The value of T'_u for the stream turbulence itself is about 0.2 at $x/h_f = 7.8$ reducing to about 0.09 around reattachment. These values span the constant value of about 0.18 measured by Kiya & Sasaki (1983) at the outer edge of the shear layer – this represents a roughly linear growth of lengthscale with x, corresponding to the scale of the large vortex structures present in the developing mixing layer.† In the latter half of the separated shear layer one might therefore anticipate some direct interaction of the FST with the mixing layer. However, figure 16 suggests that the interaction begins much earlier than this – the peak T'_u at $x/h_f = 7.8$ has already been reduced by a factor of two by the FST. In any case, these peak values are themselves very much greater than those on the edge of the flow and, as argued by CH and others, are symptomatic of a low-frequency unsteadiness associated with the relaxation from one particular shedding phase to another. Cherry *et al.* (1984) have studied this in some detail and suggested that the low-frequency motion, since it scales quite well on the reattachment length, is probably related to the overall bubble scale.

Figure 17 shows timescale data normalized by ΔU and Λ for both flows and at identical values of x/x_R (0.51, 0.95 and 1.23). Clearly the low-frequency motions do not scale exactly on 'bubble' parameters and there remains a distinct effect of FST in reducing the peak timescales. Cherry *et al.* presented surface pressure spectra

† Some of Kiya & Sasaki's (1983) measurements were made at the outer edge of the flow and a referee has pointed out that caution needs to be exercised in interpreting timescale data in a flow which contains large non-turbulent contributions to, say, the turbulence energy. Wood & Ferziger (1984) showed that the timescale of the potential motion depends on the normal distance from the turbulence. In the present case, most of the timescale measurements were made deep within the turbulent fluid, where the influence of non-turbulent contributions must be relatively insignificant.

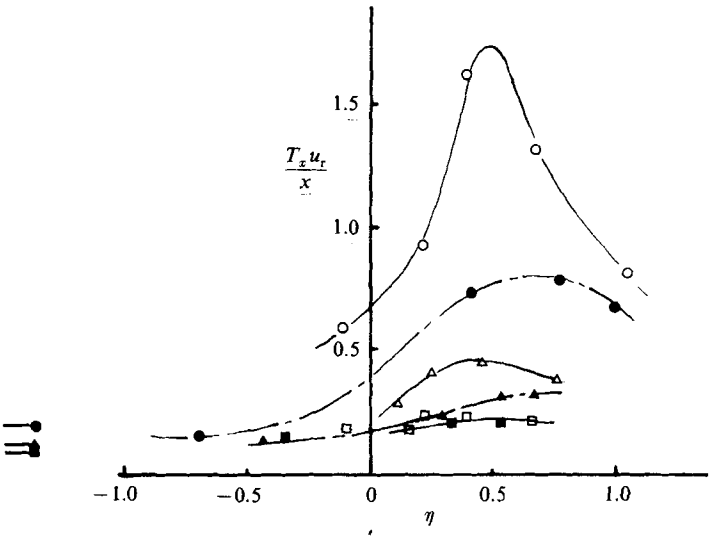

FIGURE 16. Integral timescales. $x/h_i =$: ○, ●, 7.8; △, ▲, 14.2; □, ■, 18.4. Solid and open symbols are with and without FST, respectively. Free-stream values at left.

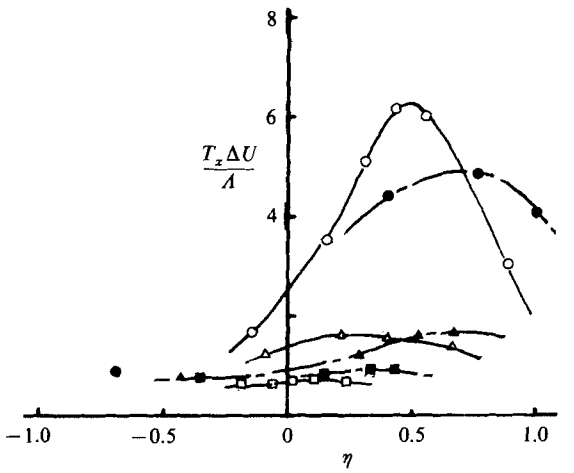

FIGURE 17. Integral timescales normalized on 'bubble' parameters. $x/x_R =$: ○, ●, 0.51; △, ▲, 0.95; □, ■, 1.23. Solid and open symbols are with and without FST, respectively.

obtained near separation ($x/x_R < 0.1$) in their case of a long blunt plate normal to uniform or turbulent streams. Although the low-frequency peak occurred near a non-dimensional frequency, nx_R/U_r, of about 0.1 in both cases, close inspection of their results does reveal a noticeable increase in this frequency in the FST cast. A significant reduction in the amount of pressure energy around that frequency, compared to that at the higher frequencies corresponding to the ordinary shear-layer scales, was also apparent. Such features were confirmed by further experiments (Hillier & Dulai 1985) which also showed that around reattachment the pressure energy spectral peaks occurred at gradually decreasing values of nx_R/U_r as the lengthscale of the free-stream turbulence increased.

These various results are summarized in figure 18, where the peak integral timescales, normalized by U_r and x_R, are plotted against x/x_R for both uniform and

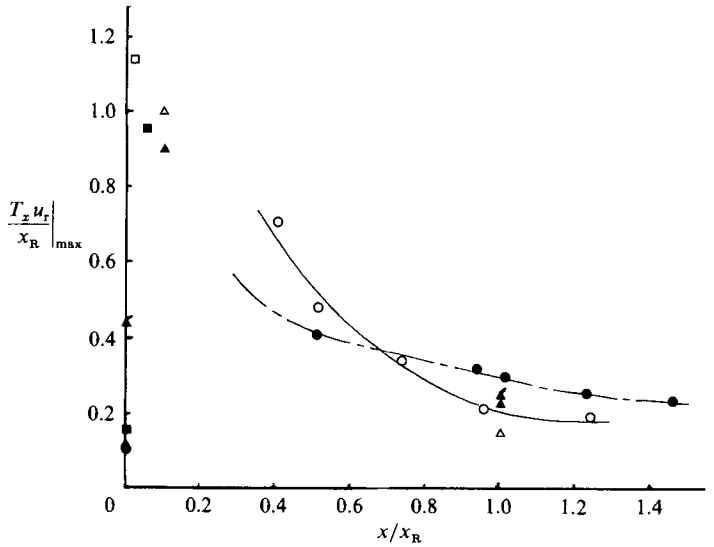

FIGURE 18. Development of peak integral timescales. ○, no FST; ●, with FST ($L_x/x_R = 0.11$). Lines added for clarity. ▲ (0.12), ◭ (0.44), △, from Hillier & Dulai (1985); ■ (0.16), □, from Cherry *et al.* (1984); open symbols are for no FST. Free-stream values of T_x (bracketed above) are for $x = 0$ and are indicated on the ordinate.

turbulent streams. Estimates from Hillier & Dulai (1985) and Cherry *et al.* (1984) are included; these have been obtained from the frequencies corresponding to pressure spectral peaks (noting that the timescale for these will be roughly 8 times that defined by equation (1) with $R(\tau)$ referring to a pressure correlation – see CH). The general trend in the present data is quite clear and is in line with the other recent work, although it should be noted that the direct comparability of timescale trends deduced from pressure and velocity spectra is only viable because it is the largest scale motions that are being considered here. FST reduces the timescale of the low-frequency 'flapping' motions most easily detected near separation. It also seems to reduce the rate at which the peak timescales fall, so that around reattachment these are actually higher than they are in the absence of FST. Figure 17 shows that whilst, in the latter case, the timescales are roughly constant across the flow at reattachment (as also found by Kiya & Sasaki 1982), they are certainly not when FST is present. In fact, in the near-wall region they are higher by at least a factor of two than those in the outer region of the flow. At the same x/h_f position, however, the T'_u variation is eventually very similar – note the data for $x/h_f = 18.4$ in figure 16.

6. Final discussion and concluding remarks

The results presented in the previous sections generally support the implications of previous work. It has been shown that free-stream turbulence leads to an increased 'flapping' motion of the shear layer just after separation, giving higher axial Reynolds stresses across the whole layer. In common with the recent findings of Hillier and his co-workers (Hillier & Cherry 1984; Cherry *et al.* 1984; Hillier & Dulai 1985) the frequency of this relatively long-timescale motion is noticeably increased. Now the integral timescales of the free-stream turbulence are in most cases studied very much lower than the timescales of the flapping motion itself. At first sight such an effect might therefore seem surprising. However, timescales based on free-stream

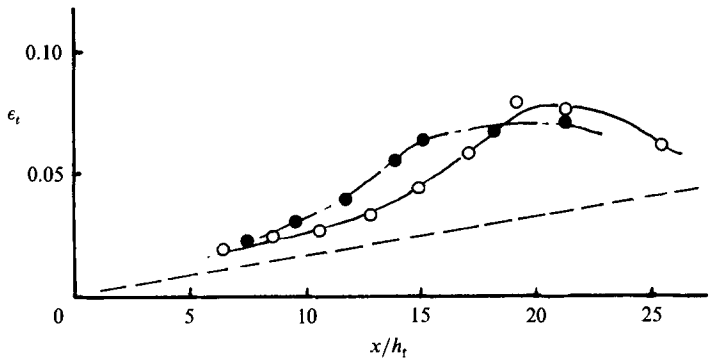

FIGURE 19. Axial development of the eddy viscosity ($-\overline{uv}/\Delta U\, h_r\, \partial U/\partial y$) along line of maximum $\overline{q^2}$. ○, no FST; ●, with FST; ———, plane mixing layer.

turbulent velocities (i.e. eddy turnover timescales), are actually comparable with the 'flapping' timescales. In the present case, although $T_x U_r/x_R$ in the free stream near separation is only about 0.1, compared with unity for the low-frequency motions, the timescale defined by using $L_e/(\overline{q^2})^{\frac{1}{2}}$ in the free stream, rather than T_x, is $O(1)$. Some direct interaction is therefore to be expected.

Entrainment rates are significantly increased by FST and by the time the shear-layer large eddy scales have become more comparable with the FST integral scales, entrainment on the lower edge of the shear layer is increased more than that on the high-velocity side. This, in turn, leads to a more rapid rise in the Reynolds stresses as reattachment is approached, even though the fluid around reattachment itself has rather lower total turbulence energy levels, at least in the near wall region. This latter result, together with the fact that the peak fluctuating pressure and wall friction levels are higher, suggests that the free-stream turbulence acts so as to concentrate the turbulence energy in the larger-scale motions. However, detailed velocity spectral measurements are needed before such arguments can be totally convincing.

A simple-minded force balance on the overall bubble would suggest that a shorter reattachment region is symptomatic of a relatively higher level of shear stress along the shear-layer centreline (since the pressure rise to reattachment seems roughly independent of x_R). The results confirm that this is, in fact, the case (figure 9) and figure 19 shows the distribution of the turbulent eddy viscosity along the line of maximum turbulence energy. This rises more rapidly in the presence of FST so the addition of the latter is, in one sense, rather like a decrease in Reynolds number in the corresponding laminar flow case. Both lead to a reduction in reattachment length because of a more rapid shear-layer growth rate.

The fact that reattachment occurs earlier means that the normal stress component ($\overline{v^2}$) cannot rise as high as it does in the absence of FST. In both cases all stresses are amplified because of a 'positive feedback' process at reattachment, but with earlier reattachment $\overline{v^2}$ saturates earlier. The turbulence structure of the flow around reattachment is consequently rather different in the two cases. In that the integral timescale varies substantially across the flow at reattachment with FST (it is roughly constant without) it is possible that the large eddy structure is also rather different, although the flow probably becomes more similar further downstream.

Further study of this large eddy structure and the way it is influenced by free-stream turbulence of various scales will be important in giving greater insight into

the nature of such separated flows. In particular, it would be helpful to measure spatial lengthscales directly and to link their development with the free-stream turbulence scales. Work is currently under way to this end, but the results from both this and the earlier study have further emphasized the complicated nature of separated flows. It would seem that their accurate prediction by any of the 'standard' turbulence models currently in use would be somewhat fortuitous.

A.H. is grateful to the Science and Engineering Research Council for support during the course of this work.

REFERENCES

BEARMAN, P. W. 1978 Turbulence effects on bluff body mean flow. *Proc. 3rd US Natl Conf. on Wind Engng, Florida*, p. LV-1.

BEARMAN, P. W. & MOREL, T. 1983 Effect of free stream turbulence on the flow around bluff bodies. *Prog. Aerospace Sci.* **20**, 97–123.

BROWN, G. L. & ROSHKO, A. 1974 On density effects and large structure in turbulent mixing layers. *J. Fluid Mech.* **64**, 775–816.

CASTRO, I. P. 1985 Time domain measurements in separated flows. *J. Fluid Mech.* **150**, 183.

CASTRO, I. P. & DIANAT, M. 1983 Surface flow patterns on rectangular bodies in thick boundary layers. *J. Wind Engng Indust. Aero.* **11**, 107.

CASTRO, I. P. & FACKRELL, J. E. 1978 A note on two-dimensional fence flows with emphasis on wall constraint. *J. Ind. Aero.* **3**, 1.

CASTRO, I. P. & HAQUE, A. 1987 The structure of a turbulent shear layer bounding a separation region. *J. Fluid Mech.* **179**, 439.

CHERRY, N. J., HILLIER, R. & LATOUR, M. E. M. P. 1984 Unsteady measurements in a separated and reattaching flow. *J. Fluid Mech.* **144**, 13.

COMPTE-BELLOT, G. & CORRSIN, S. 1966 The use of a contraction to improve the isotropy of grid-generated turbulence. *J. Fluid Mech.* **25**, 657.

HANCOCK, P. E. & BRADSHAW, P. 1983 The effect of free-stream turbulence on turbulent boundary layers. *Trans. ASME* I: *J. Fluids Engng* **105**, 284.

HILLIER, R. & CHERRY, N. J. 1981 The effects of stream turbulence on separation bubbles. *J. Wind Engng Indust. Aero.* **8**, 49.

HILLIER, R. & DULAI, B. S. 1985 Pressure fluctuations in a turbulent separated flow. *Proc. 5th Intl Symp. on Turbulent Shear Flows, Cornell.*

KIYA, M. & SASAKI, K. 1983 Structure of a turbulent separation bubble. *J. Fluid Mech.* **137**, 83.

NAKAMURA, Y. N. & OZONO, S. 1987 The effects of turbulence on a separated and reattaching flow. *J. Fluid Mech.* **178**, 477.

PATEL, R. P. 1978 Effects of stream turbulence on free shear flows. *Aero. Q.* **29**, 33.

PUI, N. K. & GARTSHORE, I. S. 1979 Measurements of the growth rate and structure in plane turbulent mixing layers. *J. Fluid Mech.* **91**, 111.

ROSHKO, A. & LAU, J. C. 1965 Some observations on transition and reattachment of a free shear layer in incompressible flow. *Proc. 1965 Heat Transfer and Fluid Mech. Inst.*

WOOD, D. & BRADSHAW, P. 1982 A turbulent mixing layer constrained by a solid surface. Part 1. Measurements before reaching the surface. *J. Fluid Mech.* **122**, 57.

WOOD, D. H. & FERZIGER, J. H. 1984 The potential flow bounded by a mixing layer and a solid surface. *Proc. R. Soc. Lond.* A**395**, 265.

WYGNANSKI, I. & FIEDLER, H. E. 1970 The two-dimensional mixing region. *J. Fluid Mech.* **41**, 327.